
DOI: 10.1002/((aelm.201800462))

Article type: Communication

A Moss-inspired Electroless Gold-Coating Strategy to Stretchable Fiber Conductor by Dry Spinning

*Yunmeng Zhao, Dashen Dong, Shu Gong, Laurence Brassart, Yan Wang, Tiance An, Wenlong Cheng**

Y. Zhao, D. Dong, Dr. S. Gong, Y. Wang, T. An, Prof. W. Cheng

Department of Chemical Engineering, Monash University, Clayton, Victoria 3800, Australia

E-mail: wenlong.cheng@monash.edu

Y. Zhao, D. Dong, Dr. S. Gong, Y. Wang, T. An, Prof. W. Cheng

The Melbourne Centre for Nanofabrication, Clayton, 151 Wellington Road, Clayton, Victoria 3800, Australia

Dr. L. Brassart

Department of Materials Science and Engineering, Monash University, VIC 3800, Australia

Keywords: stretchable, fibers, conductors, dry spinning, gold nanowires

This is the author manuscript accepted for publication and has undergone full peer review but has not been through the copyediting, typesetting, pagination and proofreading process, which may lead to differences between this version and the [Version of Record](#). Please cite this article as [doi: 10.1002/aelm.201800462](https://doi.org/10.1002/aelm.201800462).

This article is protected by copyright. All rights reserved.

Abstract

Stretchable fiber conductors are appealing in the field of soft electronics due to their potential to be woven into fabrics leading to smart textile electronics. Coating highly conductive metal films onto elastic polymer fibers can be a potential strategy, however, it is nontrivial to achieve strong metal/polymer adhesion to prevent from interfacial failure under large mechanical strains. Here, we report a novel moss-inspired gold-coating strategy by using ultrathin gold nanowires (AuNWs)-seeded electroless deposition strategy to fabricate stretchable fiber conductors in a dry spinning process. By optimizing Hildebrand's and Hansen's solubility parameter, the AuNWs are dispersed well in elastomer matrix leading to the efficient scalable production of AuNWs-impregnated elastomeric fibers. Remarkably, these AuNWs can serve as "seeds" to promote conformal electroless deposition of gold films to substantially enhance the fiber conductivity. Such gold films resemble moss exhibiting strong adhesion to elastomeric polymer fibers because they have AuNWs roots embedded in the polymer matrix. With prestrained fibers, directional cracks along axis are found but they can be repaired reversibly when strains are re-applied. This leads to substantial conductivity enhancement. Our fiber conductors can be woven into an everyday glove to exhibit superior strain-insensitivity without changing the intensity of light-emitting diode under severe deformations.

1. Introduction

Soft electronics has attracted increasing research attention over the past several years and exhibited novel applications in mechanical sensors,^[1] temperature sensors,^[2] soft conductors,^[3] energy harvesting,^[4] energy storage,^[5] implantable devices^[6] and soft displays.^[7] In many of those applications, stretchable fiber conductors are appealing because

they offer the unique advantage of unnoticeable size in wearing, scalable production and potential to be woven into the everyday fabrics. Stretchable fiber conductors usually consist of elastic fiber substrates and conductive fillers, and mixing and coating methods are two main approaches to combine elastic substrates and conductive fillers.^[8–17] However, the mixing method requires high volume ratio of conductive filler in the elastic substrate, which usually reduces elasticity;^[10,12] whereas, the coating method often raises concerns of delamination due to Young's modulus mismatch between elastomeric polymers and active materials.^[18] Furthermore, most fiber conductors reported to date experience a large decrease of conductivity under large strain because of poor control over elastomer/active materials interface.

Melt spinning and solution spinning are two scalable approaches previously reported to produce stretchable fiber conductors. The former approach can lead to highly elastic polymer fiber rapidly, but it requires high temperature to melt the raw materials, hence, limits to the scope of available suitable materials.^[8,19] Solution spinning, such as wet spinning and electrospinning, involves much milder conditions to be compatible with high-performance conductive nanofillers. Nevertheless, it requires an excessive solution to solidify fibers (e.g. wet spinning), high-voltage conditions (e.g. electrospinning). Typically, it offers poor control over properties of individual fibers.

Herein, we report on a novel dry spinning process to fabricate stretchable fiber conductors based on ultrathin gold nanowires (AuNWs). Ultrathin AuNWs were soft, flexible and analogous to polymeric chains due to small diameter (2 nm), high aspect ratio (>10,000) and good dispersibility, which has been used in various soft sensing and energy devices.^[7,20–23] The AuNWs could be well mixed with elastic styrene-ethylene-butylene-styrene (SEBS) block copolymer in THF to form a viscous and volatile spinning solution to form AuNWs/SEBS fibers in the air. Inspired by mosses, tiny plants that can attach on tree trunk firmly by penetrating their rhizoid in the tree bark, a nanowire-rooted gold/polymer interfacial design by

using AuNWs both as “roots” to attach onto and “seeds” to sprout from in an electroless deposition (ELD) process was developed. This led to “moss-like” gold film which could not only offer high conductivity (up to 461.2 S cm^{-1}), but also offered strong adhesion to SEBS polymer. This unique nanowire-rooted gold/polymer interface design explained well the highly reversible electrical responses to stretch/release cycles. Different from literature, we observed dramatic conductivity enhancement of $> 600\%$ when the fiber was stretched to 380% strain. This extraordinary increase of conductivity could be well explained by the crack-self-repairing mechanism. We further demonstrate the application of our fiber conductors for wearable and stretchable light-emitting diode (LED).

2. Results and discussion

AuNWs were synthesized according to the reported method with minor modification.^[24] To mix AuNWs and SEBS well in solution, solubility parameters were carefully investigated here to choose a compatible solvent. Developed by J. Hildebrand and C. Hansen, solubility parameter (δ) is a powerful tool for predicting if a solute will dissolve in a solvent and form a solution, and when solute and solvent share similar δ value, they can be miscible.^[25,26] The δ value of SEBS block polymer is $17.1 \text{ MPa}^{1/2}$.^[27] The solubility of the ultrathin AuNWs could be predicted by their capping molecule oleylamine ($\delta=16.6 \text{ MPa}^{1/2}$).^[28] Furthermore, due to ultrathin diameter and high aspect ratio, the behavior of AuNWs in solution can be predicted as the behavior of linear polymer chains,^[29] indicating good compatibility with linear SEBS block polymer molecules. Referred to solubility handbook and the previous publication,^[27,30] AuNWs and SEBS both could be dissolved in THF ($\delta=18.0 \text{ MPa}^{1/2}$), cyclohexane ($\delta=16.8 \text{ MPa}^{1/2}$) and toluene ($\delta=18.3 \text{ MPa}^{1/2}$).^[31] Among the three solvents, THF has the lowest boiling point (66°C), and it evaporates rapidly at room temperature providing the fastest drying speed of solution. As shown in Table S1 and Figure S1, spinning solutions using cyclohexane and toluene did not lead to formation of good fibres due to their higher boiling point.

Therefore, THF was chosen to be the solvent in the dry spinning process. A certain weight ratio of silicone oil (silicone oil/SEBS, w/w) was added to the solution as the plasticizer of SEBS. Without silicone oil, the extruded spinning solution formed beads on the needle tip and resulted in short fibers and beads of polymers. However, excess silicone oil lowered the mechanical performance of the dry spun fiber. And fibers with the 10/100 (w/w) silicone oil showed the best mechanical performance (shown in Table S1). Therefore, 10/100 (w/w) silicone oil was added into the following spinning solutions. And the elastic behavior of the SEBS fiber with 10/100 (w/w) silicone oil was evaluated and shown in Figure S2. In the loading/unloading cycles within 400% strain, the loading curve of each cycle overlapped, showing that the fiber was highly elastic in this range. And in the range from 500 to 600%, the fiber showed some hysteresis due to the viscoelasticity of the SEBS.

The formulas of the spinning solution are shown in Table S2 (Supporting information), and in this work, stretchable fibers containing 8.33, 15.4 and 21.4 wt% of AuNWs were used. Some aggregation phenomena of nanofillers in polymer solution were reported, and extra surface modifications or additive agents were used to help dispersion^[32,33]. In this work, due to the good dispersibility and flexibility, AuNWs were well mixed with SEBS polymer without the need of an extra surfactant.

Figure 1a illustrates the dry spinning process for producing the AuNWs/SEBS elastic fiber. The spinning solution was extruded out from a needle directly into the air. Due to the rapid evaporation of THF, the stream of the solution dried to form fiber directly in the air at room temperature (supporting Figure S3). As shown in Figure 1b, a dry-spun fiber longer than 10 meters was collected on a metal bobbin, showing the potential for large-scale production. The uniform dark colour indicates the uniform dispersion of AuNWs throughout the SEBS fibers. Compared to the wet spinning method, this dry spinning method does not need an extra solvent to solidify fibers; compared to the electrospinning, no high voltage is required.

The electroless deposition used to plate a gold film on the outmost surface of pre-strained AuNWs/SEBS fiber is shown in Figure 1b-e.^[34,35] We found that the AuNWs played a crucial role in the successful gold coating, for they served as “seed” to initiate nucleation/growth process.^[36] Though ultrathin AuNWs were extremely hard to be seen in the scanning electron microscope (SEM) image, the evidence of exposed AuNWs could be clearly identified in the energy-dispersive X-ray spectroscopy (EDX) mapping (Figure 1g). Evidently, gold nanowires were present throughout the SEBS fibers both inside and outside. In the initial stage of the ELD process, the deposition of gold occurred on the surface of the fiber in 10 seconds (Figure S4). After 100 seconds, a continuous layer of gold formed. With longer ELD time, the thickness of the gold film increased gradually up to about 200 nm in 10 minutes (Figure S5). After ELD, black fibers became golden (Figure 1h) demonstrating the formation of conformally coated gold film (Figure 1j). This shows the formation of moss-like gold nanofilms with planted gold nanowires inside SEBS fibers. It is well known that mosses grow from spores and penetrate their thin, long and threadlike rhizoids into the substrate to attach them firmly on slopping and vertical surfaces. Analogous to the conformal moss grown on woods or soil, our gold coated films have AuNWs as “root” embedded in the SEBS fiber. Such moss-like gold films showed good adhesion to the SEBS fiber and could survive in the polyimide tape test without obvious conductivity loss (shown in Video S1, Supporting Information). This may be because AuNWs embedded in the polymer matrix behave like “roots”.

To further prove the important role of the AuNWs, a set of control experiments using the same weight percentage of gold nanoparticles (AuNPs) instead of AuNWs was conducted. Both AuNWs and AuNPs are capped by oleylamine and their transmission electron microscope (TEM) image is shown in **Figure 2a-b**, respectively. Compared to spherical AuNPs, AuNWs are entangled similar to polymer chains (Figure 2c-d),^[37] which led to a negligible change of elasticity of SEBS fibers. As shown in Figure 2e, the addition of AuNWs gave rise to an increase of 75% of the tensile strength compared to the pure SEBS fiber, and

only exhibited a negligible decrease in breaking strain (red line in Figure 2e). In contrast, the addition of AuNPs decreased tensile strength and elasticity of the fibers (blue line in Figure 2e). In addition, a continuous layer of gold film could be achieved on the surface of the AuNWs/SEBS fiber, but not for the surface of the AuNPs/SEBS fiber (Figure 2f). This could be due to the low coverage of AuNPs on the fiber surface with low ELD efficiency as evidenced from dark color (Figure 2f).

We also carefully examined how the complexing agents influenced the ELD process. Note that the nucleation and reduction could occur undesirably in the solution, and 4-mercaptobenzoic acid (MBA) was chosen to restrain the rate of the reactions in the solution due to strong bonding and confinement between its thiol group and gold atom.^[34] Consequently, the ELD process occurred site-selectively on the AuNWs “seed” forming a uniform gold film. In control experiments without adding MBA or using a weak complexing agent cetyltrimethylammonium chloride, the ELD solutions turned purple color, indicating uncontrollable nucleation and reduction of gold in the bulk solution (Figure S6). Consequently, strong golden reflection film couldn't be obtained (Figure S7).

To further enhance conductivity, a room-temperature wet nanowelding approach was used to remove MBA ligands.^[38] After the ELD process, the fibers were washed thoroughly with water and then immersed in the NaBH_4 solution for 10 minutes. The hydride derived from NaBH_4 solution provides a much stronger binding affinity so that thiol groups will be easily replaced by hydride.^[38] Both hydride and NaBH_4 eventually decomposed in water, and all residues could be removed completely, as proved by Raman spectra (Figure S8 and Figure S9). The nanowelding step led to the fusion of gold islands into a mechanically strong gold film. Without this step, the gold film ruptured into discrete islands after the fiber was released from solution (Figure S10). Consistent with this, the conductivity of the fiber with wet nanowelding step was significantly improved (Figure S11).

As expected, wrinkled structures were observed upon releasing pre-straining with a gold film formed in the last releasing step of the fabrication process, shown in Figure 1e. As described above, the gold film was grown on the exposed AuNWs, and the connection between AuNWs and gold film prevented complete delamination during releasing. Consequently, the gold film was forced to fold and wrinkle with some parts strongly adhered to the AuNWs seeds. Simultaneously, due to positive Poisson's ratio of SEBS (0.49),^[39] the cross-section of fiber expanded during releasing, and the gold film was forced to crack along the axis. Finally, periodically wrinkled and cracked gold film form on the surface of the fiber.

The electrical performance was largely affected by the pre-strains applied in the ELD and nanowelding process. **Figure 3a** shows the normalized resistance change curves of the stretchable conductive fiber prepared with different pre-strains while keeping the same weight ratios of AuNWs in fiber and durations of ELD (21.4 wt% and 10 min, respectively). Clearly, not only did large pre-strain enhance stretchability but also made the resistance insensitive to strain. The resistance of the 600% pre-strained fiber increased only 210% when 380% strain was applied. We further compared the fiber conductivities which were calculated using the following equation [1].

$$S = \frac{L}{A \times R} \quad [1]$$

Where S is the conductivity of the stretchable conductive fiber, L is the length of the fiber, A is the cross-section area of the fiber, and R is the resistance of the fiber. The length and the cross-section area of the fiber to be used in the equation were measured at every 20% strain, the cross-sectional areas corresponding to the strain were shown in Figure S12. The initial conductivities of fibers with different pre-strains were similar around 60 to 100 S cm⁻¹, but their conductivity-strain curve differed significantly. With 100% and 200% pre-strain, the conductivity decreased with the strain. But 300% and 600% pre-strained fiber' conductivities exhibited increased with the strain. The highest conductivity 461 S cm⁻¹ was achieved by the pre-strained 600% fiber at the maximum strain 380% with 642% conductivity enhancement.

The reason for the mismatch between the applied pre-strain level and conductive strain range can be found by analyzing the stretching process of the gold film and AuNWs/SEBS fiber. During the last releasing step of fabrication, the wrinkling deformation of the gold film was driven by the retraction of AuNWs/SEBS fiber but simultaneously the rigid gold films prevented the full recovery of the SEBS fiber to its original length. Consequently, the length of the stretchable fiber conductor was longer than the as-spun AuNWs/SEBS fiber. Therefore, the conductive strain range was smaller than the pre-strain level applied in the fabrication.

Furthermore, we found that AuNWs loading in SEBS fibers played a minor role in the overall conductivity. Figure 3c shows the conductivity-strain curves of fibers with three different AuNWs loading (all pre-strained 300% and 10 min ELD). These curves exhibit similar trends with comparable values, demonstrating that it was the outmost gold film on the surface that governed the overall conductivity.

We also evaluated the effects of ELD times on mechatronic properties (Figure 3d). It appeared that ELD time had no influence on the trend that conductivity increased with the strain. The initial conductivity of the fibers with deposition time from 2 to 10 min increased from 27 to 92 S cm⁻¹ (Figure S13), demonstrating that longer ELD time typically led to high conductivities. However, fiber with ELD longer than 10 min typically failed under large strains (Figure S14). This was because thick gold coating increased the rigidity of fibers.

We plotted the normalized conductivity-strain curves for our stretchable fiber conductors and those obtained by wet spinning in the literature (Figure 3e). Interestingly, only our fiber conductors exhibit increased conductivity as the strain level is increased, and all the reported wet-spun fibers showed an opposite trend. Although our fiber's absolute conductivity wasn't high at 0% strain when compared to literature, it surpassed those reported conductivities when strain level was over ~150% strain (Figure 3f).

To investigate the underlying mechanism for the aforementioned unconventional mechanical properties of our fiber conductors, their surface morphologies under pre-strain-releasing-stretching cycles was characterized *in-situ* by SEM. For 300% pre-strained fiber, no surface cracks could be observed (**Figure 4a**); upon full strain release to 0% strain, the gold film cracked and wrinkled (**Figure 4b**). The cracks can be attributed to expansion in the transverse directions during strain release; whereas the wrinkling is due to compression in the longitudinal direction. When the fiber was re-stretched from 0 to 200% strain, the wrinkles gradually disappeared, and the cracks gradually repaired by themselves (**Figure 4b-d**). In this process, the fiber conductor undertook axial expansion and radial compression, which are responsible for smoothening wrinkles and self-repairing of cracks, respectively. At 200% strain, we almost recovered a smooth gold film on the fiber surface. This crack-repairing process explains well why our fibers' conductivity increases under strain. It is fundamentally different from percolation-based principle reported in the literature.^[9–12,40]

To evaluate the reliability and durability of our stretchable fiber, the resistance change was measured under dynamic and continuous stretching releasing cycles. **Figure 5a** shows normalized resistance change curves of a pre-strained 300% conductive fiber under 100%, 150%, and 200% stretching-releasing cycles. The nearly symmetrical curves indicate that the change of fiber' resistance was nearly reversible without obvious hysteresis. It is noteworthy that the first half parts of three curves overlap each other, indicating the great reliability to endure dynamic stretching. The stretchable conductive fibers are also highly durable with stable signal and baseline levels for 5000 cycling test (**Figure 5b**). After the 4-hour-cycling test, the line shape for the last 10 cycles retained almost identical to that for the first 10 cycles (**Figure 5c**). Besides, the surface morphology of the stretchable fiber conductor before and after the 5000-cycle durability test was characterized by SEM and shown in **Figure S15**. Note that the gold film still attached firmly on the surface of the fiber after hours of stretching/releasing cycles. This demonstrates the strong adhesion between the gold film to the SEBS fiber.

Our stretchable fibers could be woven into everyday fabrics as illustrated in Figure 5d. As a proof of concept, a stretchable conductive fiber was woven in a glove as a part of a wearable light-emitting diode (LED) circuit without influencing the glove's overall appearance (Figure 5e). Powered by a 12V DC voltage, constant illumination was emitted when the glove was severely stretched and bent (Figure 5f-g and Video S2, Supporting information). It demonstrated the potential application of our fiber conductors in wearable textile electronics. Stable LED light intensity was maintained during severe stretching and bending as shown in the Video S2. We have also done the knotting test which involved in sever twisting and other mechanical deformation. As the proof of concept, 10 knots were made to compare the conductivity before and after knotting (Figure S16). Note that the resistance of the fiber increased only 10% with 10 knots, exhibiting potential applications in textile electronics.

3. Conclusion

In summary, we reported a simple yet efficient dry spinning method to produce a stretchable conductive fiber with Moss-inspired gold/elastomer interface design. Compared to reported polymer solution spinning methods such as wet spinning and electrospinning, the dry spinning process uses much less solvent without the need of expensive instrument. The conductivity of the fiber was enhanced by the gold film grown on the AuNWs "seeds" exposed on the surface, and the mechanical strength was enforced by the AuNWs "roots" embedded in the polymer matrix. The fiber conductors showed increasing conductivity with increasing strain, and the highest conductivity reached 461 S cm^{-1} at the maximum strain of 380%. This working mechanism could be well explained by the self-repairing of the cracked gold film during the stretching process. The low-cost fabrication, in conjunction with outstanding performance described above, indicates the potential of our methodology in wearable textile electronics.

4. Experimental section

Materials: Gold (III) chloride trihydrate ($\text{HAuCl}_4 \cdot 3\text{H}_2\text{O}$) ($\geq 99.9\%$, Sigma-Aldrich), oleylamine (OA) (70%, Sigma-Aldrich), triisopropylsilane (TIPS) (98%, Sigma-Aldrich), styrene-ethylene/butylene-styrene (SEBS) (G1651H, Kraton), silicone oil (Sigma-Aldrich), 4-Mercaptobenzoic acid (MBA) (90%, Sigma-Aldrich), L-ascorbic acid ($\geq 99\%$, Sigma-Aldrich), sodium borohydride (NaBH_4) ($\geq 98.0\%$, Sigma-Aldrich), n-hexane (GR, Merck), toluene (GR, Merck) and tetrahydrofuran (THF) (HPLC, Thermo Fisher Scientific).

Characterization: Micromorphology characterization was performed on a Philips CM20 TEM at 200 kV and an FEI Helios Nanolab 600 FIB-SEM at 5 kV and 86 pA. The stress-strain curve was obtained by a motorized test stand system (ESM301 test stand and Series 7 force gauge, MARK-10). Stretching tests were done on a motorized moving stage (Model LTS150/M, THORLABS) with two grips to hold the sample. Electrical signals were collected by an electrochemical system (VersaSTAT 3, Princeton Applied Research). To measure cross-section area, the fibers were sealed in epoxy resin for every 20% strain, and a lab knife was used to cut it into thin slices which were used to measure cross-section area by an optical microscope (Nikon ECLIPSE LV150 microscope with a Nikon Digital Sight DS-Fi1 camera). DC power was supplied by a source meter (Keithley 2400), which provided a constant 12 V voltage and maximum 100 mA current. Stainless wires and silver paste were used to stably connecting sample to the electrochemical system and source meter.

Synthesis of ultrathin gold nanowires (ultrathin AuNWs): AuNWs are synthesized following a reported method.^[24] 44mg of $\text{HAuCl}_4 \cdot 3\text{H}_2\text{O}$, 1.5mL of OA and 2.1mL of TIPS were added into 22mL hexane. The solution was kept in dark place for 2 days without stirring at room temperature to form a dispersion of AuNWs (1.10 mg mL^{-1}). This procedure could be multiplied by the same ratio of chemicals. To remove excess OA, the AuNWs was cleaned

with a mixed solvent of hexane and ethanol (3/1, v/v) and centrifuged three times, and finally re-dispersed into 5 mL of THF.

Synthesis of oleylamine capped gold nanoparticles (AuNPs): The AuNPs were synthesized following a reported method.^[41] A solution of 100 mg of $\text{HAuCl}_4 \cdot 3\text{H}_2\text{O}$ and 2.4 mL oleylamine in 2.0 mL of toluene was injected into a boiling solution of 5.8 mL oleylamine in 98 mL toluene, and the mixed solution was heated for 2 hours. 300 mL of ethanol was added to precipitate the AuNPs. The AuNPs was cleaned with 40 mL of ethanol and precipitated by centrifugation three times. And finally, AuNPs were re-dispersed into 2 mL of THF.

Dry spinning process: The first step of dry spinning was preparing a spinning solution consisting of AuNWs and SEBS. A certain weight ratio of silicone oil (silicone oil/SEBS, 10/100, w/w) was added to the solution as the plasticizer of SEBS. Referred to Table S2, spinning solution was added to a 5 mL glass vial, and shaken at 2000 rpm for 48 h on an orbital shaker, to get well dispersed. Secondly, the spinning solution was transferred into a syringe with a gauge 25 needle (inner diameter 0.260 mm). Then the syringe was fixed on a vertically placed syringe pump with its needle downward in the air. Under about 8 to 10 cm underneath the needle tip, a board covered by polyimide tape was placed. Finally, the plunger of the syringe was continuously pushed at a rate of 4 mL h^{-1} by the pump. Once the spinning solution was extruded out, the THF rapidly evaporated and the solution dried directly in the air and a fiber was formed. The fiber was collected on the board and further collected on the bobbin by hand.

Electroless deposition (ELD) and wet nanowelding process: Before the ELD, fibers were pre-strained to different percentages and fixed at two ends by tape in a long container. The electroless deposition solution was prepared based on a reported method.^[34,35] 2.4 mL of ethanol, 2.64 mL of HAuCl_4 aqueous solution (492 mg $\text{HAuCl}_4 \cdot 3\text{H}_2\text{O}$ in 50 mL water) and 0.1 mL of MBA ethanol solution (94.2 mg in 10 mL ethanol) were mixed. Then 0.4 mL of L-AA aqueous solution (710 mg in 10 mL water) was added to the previous solution and shaken by

hand for a few seconds, and rapidly poured into the long container to immerse the fibers for desired minutes. At last the ELD solution was discarded and fibers were washed with water for three times to remove residue solution. The following wet nanowelding process was based on a reported method^[37]. The fibers after ELD were immersed in 25 mM NaBH₄ water solution for 10 minutes, and then washed with water for three times and dried in air for 2 hours. At last, the pre-strained fibers were carefully released and ready to be used.

Resistance and strain measurement: The two ends of stretchable conductive fiber were fixed to the motorized moving stage by two grips. And the ends were connected to the electrochemical system. The motorized moving stage moved horizontally at configured speeds to stretch and release the fiber, and simultaneously changes of current were recorded by the electrochemical system in a potentiostatic mode. Resistance was calculated by voltage and current.

Demonstration of the stretchable fiber conductor: A conductive stretchable fiber was woven into the finger area of an elastic glove and one end of it was connected to a LED circuit that was fixed on the glove by double-sided tape. Two stainless steel wires were used to connect the fiber and LED to a source meter. A constant 12V DC voltage was applied to the LED circuit.

Supporting Information

Supporting Information is available from the Wiley Online Library or from the author.

Acknowledgments

This work is financially supported by ARC Discovery projects DP180101715 and DP170102208. This work was performed in part at the Melbourne Centre for Nanofabrication (MCN) in the Victorian Node of the Australian National Fabrication Facility (ANFF). Yunmeng Zhao acknowledge partial sponsorship for his PhD studies, and Tiance An thanks the financial aid from Chinese Scholarship Council (CSC).

Received: ((will be filled in by the editorial staff))

Revised: ((will be filled in by the editorial staff))

Published online: ((will be filled in by the editorial staff))

References

- [1] C. Pang, J. H. Koo, A. Nguyen, J. M. Caves, M. G. Kim, A. Chortos, K. Kim, P. J. Wang, J. B. H. Tok, Z. Bao, *Adv. Mater.* **2015**, *27*, 634.
- [2] S. Y. Hong, Y. H. Lee, H. Park, S. W. Jin, Y. R. Jeong, J. Yun, I. You, G. Zi, J. S. Ha, *Adv. Mater.* **2016**, *28*, 930.
- [3] Y. Tang, S. Gong, Y. Chen, L. W. Yap, W. Cheng, *ACS Nano* **2014**, *8*, 5707.
- [4] Y. Yang, G. Zhu, H. Zhang, J. Chen, X. Zhong, Z. H. Lin, Y. Su, P. Bai, X. Wen, Z. L. Wang, *ACS Nano* **2013**, *7*, 9461.
- [5] X. Chen, L. Qiu, J. Ren, G. Guan, H. Lin, Z. Zhang, P. Chen, Y. Wang, H. Peng, *Adv. Mater.* **2013**, *25*, 6436.
- [6] S. W. Hwang, H. Tao, D. H. Kim, H. Cheng, J. K. Song, E. Rill, M. A. Brenckle, B. Panilaitis, S. M. Won, Y. S. Kim, Y. M. Song, K. J. Yu, A. Ameen, R. Li, Y. Su, M. Yang, D. L. Kaplan, M. R. Zakin, M. J. Slepian, Y. Huang, F. G. Omenetto, J. A. Rogers, *Science* **2012**, *337*, 1640.

- [7] S. Gong, Y. Zhao, L. W. Yap, Q. Shi, Y. Wang, J. A. P. B. Bay, D. T. H. Lai, H. Uddin, W. Cheng, *Adv. Electron. Mater.* **2016**, *2*, 1600121.
- [8] S. Zhu, J. H. So, R. Mays, S. Desai, W. R. Barnes, B. Pourdeyhimi, M. D. Dickey, *Adv. Funct. Mater.* **2013**, *23*, 2308.
- [9] M. Z. Seyedin, J. M. Razal, P. C. Innis, G. G. Wallace, *Adv. Funct. Mater.* **2014**, *24*, 2957.
- [10] R. Ma, J. Lee, D. Choi, H. Moon, S. Baik, *Nano Lett.* **2014**, *14*, 1944.
- [11] R. Ma, B. Kang, S. Cho, M. Choi, S. Baik, *ACS Nano* **2015**, *9*, 10876.
- [12] S. Lee, S. Shin, S. Lee, J. Seo, J. Lee, S. Son, H. J. Cho, H. Algadi, S. Al-Sayari, D. E. Kim, T. Lee, *Adv. Funct. Mater.* **2015**, *25*, 3114.
- [13] Z. Xu, Z. Liu, H. Sun, C. Gao, *Adv. Mater.* **2013**, *25*, 3249.
- [14] A. J. Granero, P. Wagner, K. Wagner, J. M. Razal, G. G. Wallace, M. In Het Panhuis, *Adv. Funct. Mater.* **2011**, *21*, 955.
- [15] H. Jin, N. Matsuhisa, S. Lee, M. Abbas, T. Yokota, T. Someya, *Adv. Mater.* **2017**, *29*, 1605848.
- [16] J. Ge, L. Sun, F. R. Zhang, Y. Zhang, L. A. Shi, H. Y. Zhao, H. W. Zhu, H. L. Jiang, S. H. Yu, *Adv. Mater.* **2016**, *28*, 722.
- [17] Z. Liu, D. Qi, G. Hu, H. Wang, Y. Jiang, G. Chen, Y. Luo, X. J. Loh, B. Liedberg, X. Chen, *Adv. Mater.* **2018**, *30*, 1704229.
- [18] S. Gong, W. Cheng, *Adv. Electron. Mater.* **2017**, *3*, 1600314.
- [19] Z. F. Liu, S. Fang, F. A. Moura, J. N. Ding, N. Jiang, J. Di, M. Zhang, X. Lepró, D. S. Galvão, C. S. Haines, N. Y. Yuan, S. G. Yin, D. W. Lee, R. Wang, H. Y. Wang, W. Lv,

- C. Dong, R. C. Zhang, M. J. Chen, Q. Yin, Y. T. Chong, R. Zhang, X. Wang, M. D. Lima, R. Ovalle-Robles, D. Qian, H. Lu, R. H. Baughman, *Science* **2015**, *349*, 400.
- [20] Y. Chen, O. Zi, M. Gu, W. Cheng, *Adv. Mater.* **2013**, *25*, 80.
- [21] S. Gong, D. T. H. Lai, B. Su, K. J. Si, Z. Ma, L. W. Yap, P. Guo, W. Cheng, *Adv. Electron. Mater.* **2015**, *1*, 1400063.
- [22] S. Gong, Y. Zhao, Q. Shi, Y. Wang, L. W. Yap, W. Cheng, *Electroanalysis* **2016**, *28*, 1298.
- [23] M. D. Ho, Y. Ling, L. W. Yap, Y. Wang, D. Dong, Y. Zhao, W. Cheng, *Adv. Funct. Mater.* **2017**, *27*, 1700845.
- [24] H. Feng, Y. Yang, Y. You, G. Li, J. Guo, T. Yu, Z. Shen, T. Wu, B. Xing, *Chem. Commun.* **2009**, 1984.
- [25] J. H. Hildebrand, R. L. Scott, *The Solubility of Nonelectrolytes*, Reinhold Pub. Corp., New York, USA, **1950**.
- [26] C. M. Hansen, *Hansen solubility parameters: a user's handbook*, CRC Press, Boca Raton, USA, **2007**.
- [27] G. Ovejero, P. Pérez, M. D. Romero, I. Díaz, E. Díez, *Eur. Polym. J.* **2009**, *45*, 590.
- [28] A. E. Di Mauro, M. Striccoli, N. Depalo, E. Fanizza, L. Cano, C. Ingrosso, A. Agostiano, M. L. Curri, A. Tercjak, *Soft Matter* **2014**, *10*, 1676.
- [29] Y. Chen, Y. Wang, J. Peng, Q. Xu, J. Weng, J. Xu, *ACS Nano* **2017**, *11*, 2756.
- [30] B. Reiser, D. Gerstner, L. Gonzalez-Garcia, J. H. M. Maurer, I. Kanelidis, T. Kraus, *Phys. Chem. Chem. Phys.* **2016**, *18*, 27165.
- [31] Y. Ogata, T. Mogi, Y. Makita, *J. Polym. Sci. Part B Polym. Phys.* **2010**, *48*, 588.

- [32] R. Ma, S. Kwon, Q. Zheng, H. Y. Kwon, J. Il Kim, H. R. Choi, S. Baik, *Adv. Mater.* **2012**, *24*, 3344.
- [33] J. T. Han, S. Choi, J. I. Jang, S. K. Seol, J. S. Woo, H. J. Jeong, S. Y. Jeong, K.-J. Baeg, G.-W. Lee, *Sci. Rep.* **2015**, *5*, 9300.
- [34] J. He, Y. Wang, Y. Feng, X. Qi, Z. Zeng, Q. Liu, W. S. Teo, C. L. Gan, H. Zhang, H. Chen, *ACS Nano* **2013**, *7*, 2733.
- [35] Y. Wang, S. Gong, D. Gómez, Y. Ling, L. W. Yap, G. P. Simon, W. Cheng, *ACS Nano* **2018**, DOI 10.1021/acsnano.8b04748.
- [36] K. J. Si, Y. Chen, Q. Shi, W. Cheng, *Adv. Sci.* **2018**, *5*, 1700179.
- [37] M. A. L. Manchado, L. Valentini, J. Biagiotti, J. M. Kenny, *Carbon* **2005**, *43*, 1499.
- [38] S. M. Ansar, F. S. Ameer, W. Hu, S. Zou, C. U. Pittman, D. Zhang, *Nano Lett.* **2013**, *13*, 1226.
- [39] D. Dompas, G. Groeninckx, *Polymer* **1994**, *35*, 4743.
- [40] M. Park, J. Im, M. Shin, Y. Min, J. J. Park, H. Cho, S. Park, M.-B. Shim, S. Jeon, D.-Y. Chung, J. Bae, J. J. Park, U. Jeong, K. Kim, *Nat. Nanotechnol.* **2012**, *7*, 803.
- [41] H. Hiramatsu, F. E. Osterloh, *Chem. Mater.* **2004**, *16*, 2509.

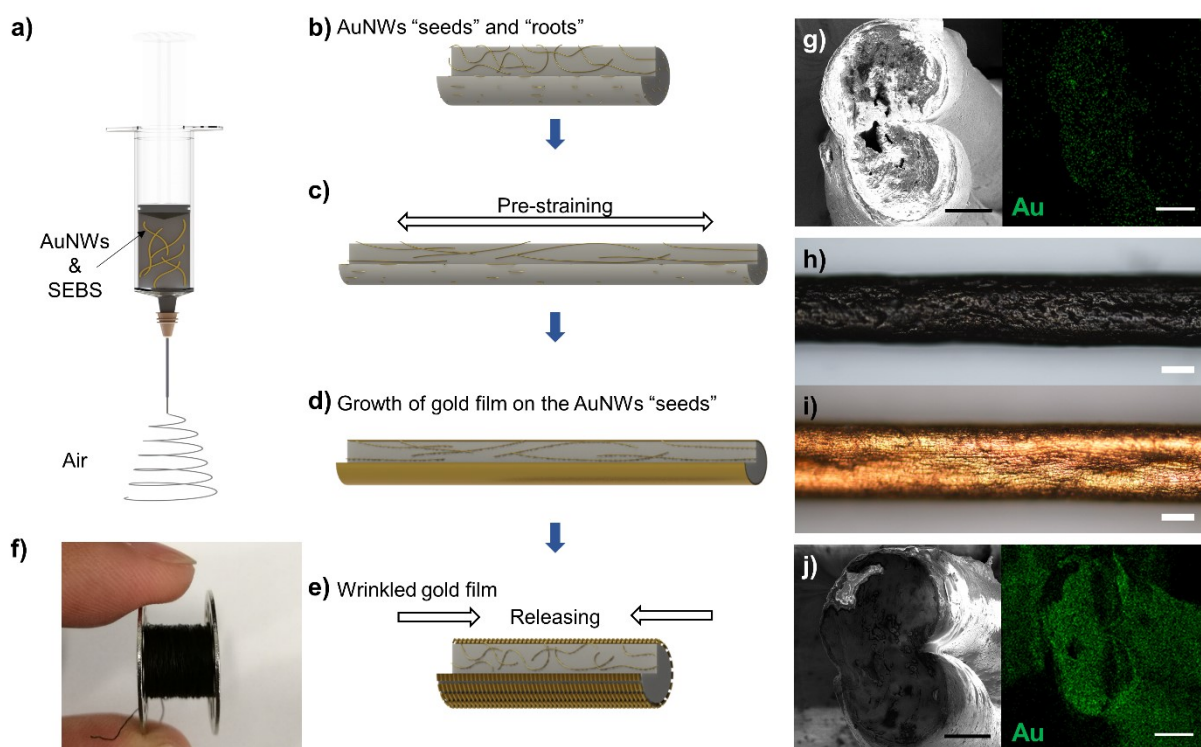


Figure 1. Schematic illustration of the fabrication process and the characterization of the dry spun stretchable fiber conductor based on ultrathin AuNWs. a) Schematic illustration of the dry spinning process to fabricate AuNWs/SEBS fiber. b-e) Schematic illustrations of the formation of AuNWs-rooted continuous gold films on the fiber surface. The embedded nanowire root in combination with the coated gold film is similar to moss structure. f) Photograph of a long AuNWs/SEBS fiber (over 10 meters) collected on a metal bobbin. g, j) Cross-sectional SEM image and EDX mapping of Au obtained from an 8.33 wt% AuNWs/SEBS fiber before and after the growth of the gold film, respectively. h-i) The optical microscope image of the AuNWs/SEBS before and after the growth of gold film, respectively. Scale bars: 100 μm .

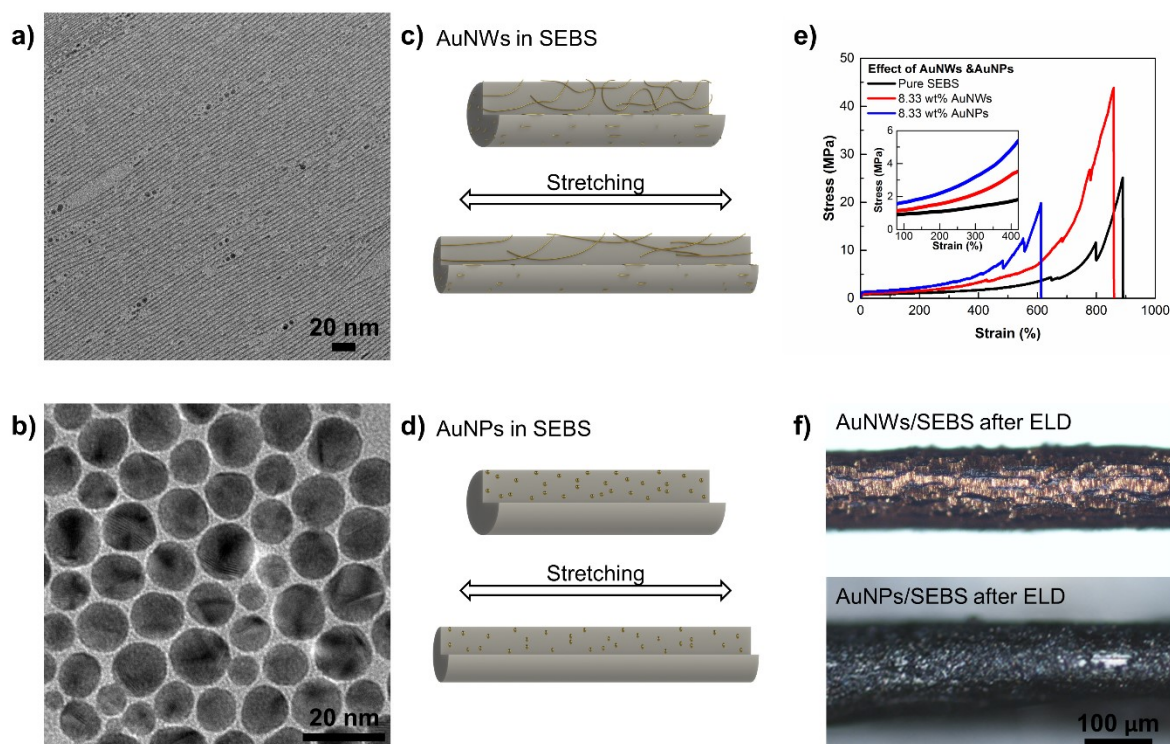


Figure 2. Characterization and schematic illustrations of the AuNWs/SEBS fiber and the AuNPs/SEBS fiber. a) TEM image of the ultrathin AuNWs and the AuNPs, respectively. c-d) Schematic illustrations of original and stretched AuNWs/SEBS fiber and AuNP/SEBS fiber, respectively. e) Stress-strain curves of pure SEBS fiber, AuNWs/SEBS fiber, and AuNPs/SEBS fiber. The inset is a zoomed-in figure of e) to show the elastic regions of the fibers. f) Optical microscope image of the AuNWs/SEBS fiber and the AuNPs/SEBS fiber after growth of gold film, respectively.

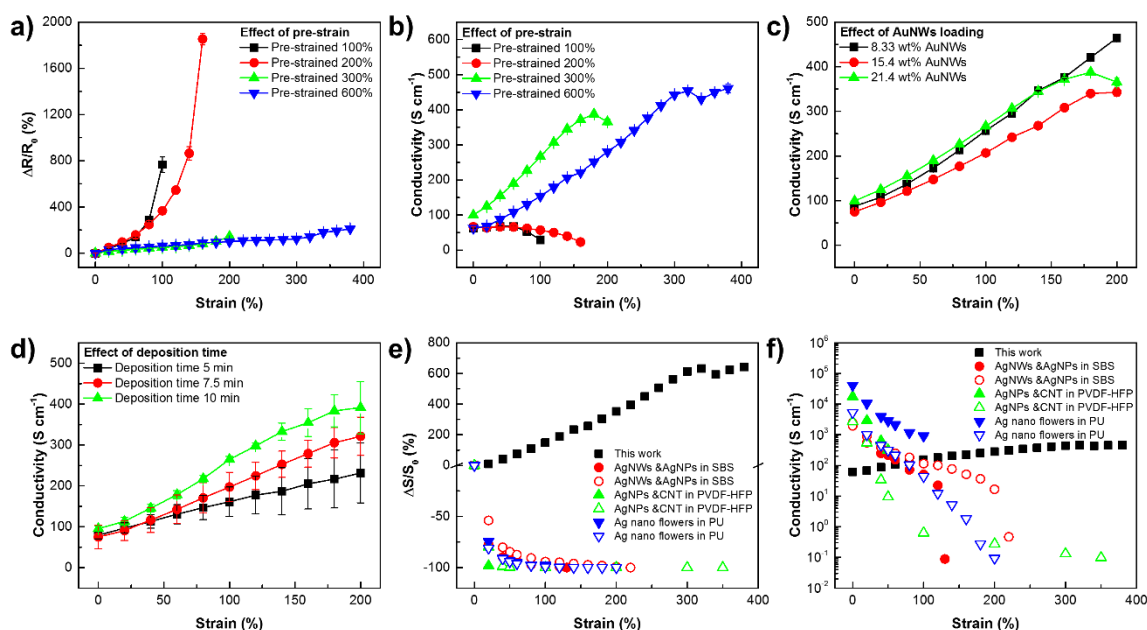


Figure 3. The electrical properties of the stretchable conductive fibers as a function of the axial strain. a) The normalized resistance change-strain curves on the effect of pre-strain levels. b) The conductivity-strain curves on the effect of pre-strain levels. c) The conductivity-strain curves on the effect of AuNWs loading in the fiber. d) The conductivity-strain curves on the effect of the gold deposition time. e) Normalized conductivity change-strain curves of our dry spun stretchable fiber conductor in comparison to reported wet spun stretchable fiber conductors. f) Conductivity-strain curves of the dry spun stretchable fiber conductor in comparison to reported wet spun stretchable fiber conductors.

●○[12], ▲△[10], ▼▽[11].

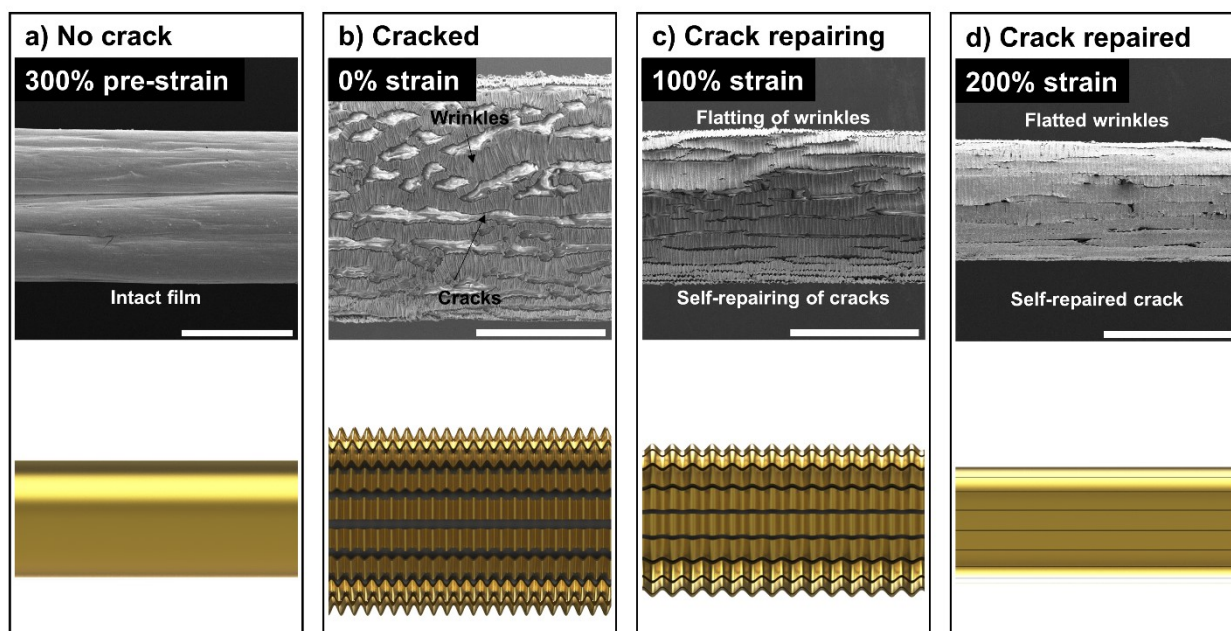


Figure 4. *In situ* SEM studies on Moss-like gold film cracking and crack repair process. a-d) SEM images and schematic illustrations of a conductive stretchable fiber under 300% pre-strain, released 0%, re-stretched to 100% and 200% strain, respectively. Scale bars: 100 μm .

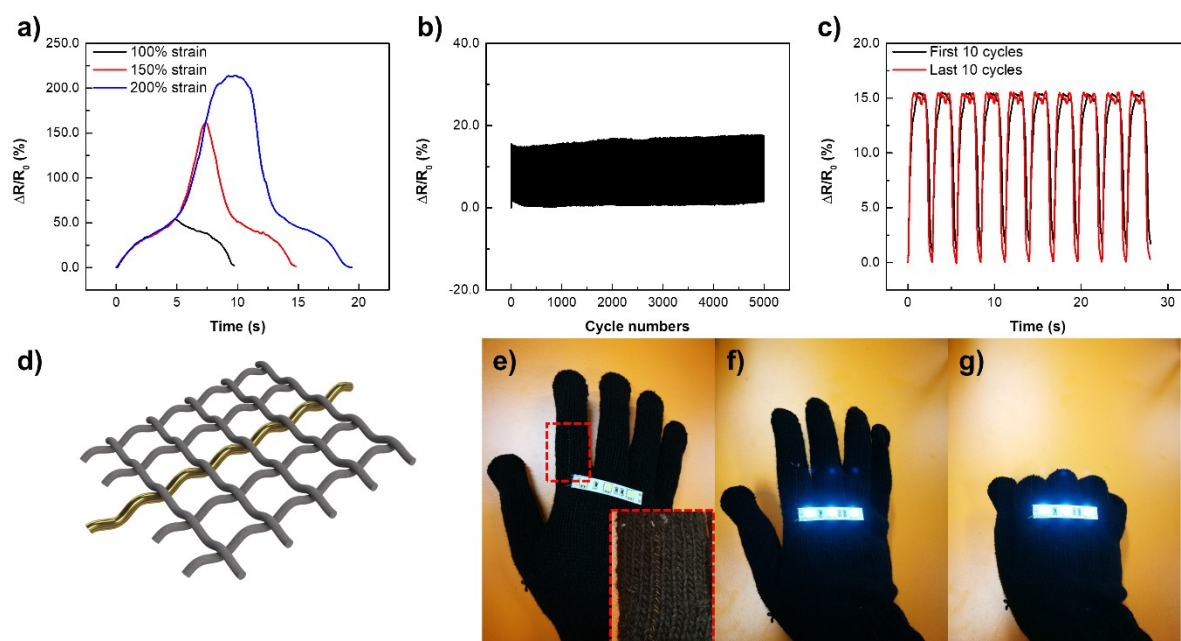


Figure 5. The durability test and demonstration of wearable LED. a) The normalized resistance change curves of a 300% pre-stained stretchable conductive fiber for the 100%, 150% and 200% stretching-releasing cycles. b) The durability test of the stretchable conductive fiber under 50% strain for 5000 cycles. 600% pre-strain was applied. c) The comparison between normalized resistance change curves for the first 10 cycles and last 10 cycles in the durability test in **b**. d) The schematic illustration of a conductive stretchable fiber woven in a piece of fabric. e) Digital photographs of a conductive stretchable fiber woven in the finger area of a black glove as a part of a wearable LED circuit.

A moss-inspired stretchable fiber conductor is fabricated in a dry spinning process together with a following ultrathin gold nanowires (AuNWs)-seeded electroless deposition process. A seed-root interfacial design of AuNWs and polymer enables the growth of gold films to enhance conductivity. And the conductivity extraordinarily increases with the increase of strain in a large range, exhibiting significant potentials in wearable devices.

Keyword stretchable, fibers, conductors, dry spinning, gold nanowires

Y. Zhao, D. Dong, Dr. S. Gong, Y. Wang, T. An, W. Cheng*

A Moss-inspired Electroless Gold-Coating Strategy to Stretchable Fiber Conductor by Dry Spinning

ToC figure

